LAWRENCE
LIVERMORE
NATIONAL
LABORATORY

UCRL-CONF-154963

Optical propagation modeling for the National Ignition Facility

W. H. Williams, J. M. Auerbach, M. A. Henesian, K. S. Jancaitis, K. R. Manes, N. C. Mehta, C. D. Orth, R. A. Sacks, M. J. Shaw, C. C. Widmayer

January 12, 2004

Photonics West – Lasers and Applications in Science and Technology (LASE) 2004
San Jose, California, January 24-29, 2004

Optical propagation modeling for the National Ignition Facility

Wade H. Williams*, Jerome M. Auerbach, Mark A. Henesian, Kenneth S. Jancaitis, Kenneth R. Manes, Naresh C. Mehta, Charles D. Orth, Richard A. Sacks, Michael J. Shaw, C. Clay Widmayer
Lawrence Livermore National Laboratory, 7000 East Ave., Livermore, CA 95336

This work was performed under the auspices of the U.S. Department of Energy by University of California, Lawrence Livermore National Laboratory under Contract W-7405-Eng-48.

ABSTRACT

Optical propagation modeling of the National Ignition Facility has been utilized extensively from conceptual design several years ago through to early operations today. In practice we routinely (for every shot) model beam propagation starting from the waveform generator through to the target. This includes the regenerative amplifier, the 4-pass rod amplifier, and the large slab amplifiers. Such models have been improved over time to include details such as distances between components, gain profiles in the laser slabs and rods, transient optical distortions due to the flashlamp heating of laser slabs, measured transmitted and reflected wavefronts for all large optics, the adaptive optic feedback loop, and the frequency converter. These calculations allow nearfield and farfield predictions in good agreement with measurements.

1. INTRODUCTION

The National Ignition Facility (NIF) is a large laser system currently under construction at Lawrence Livermore National Laboratory in Livermore, California. When completed it will house 192 laser beams capable of being focused to a common target inside a 10 meter diameter target chamber. Each beam will be approximately 370 x 370 mm square in size, with peak powers of 5-6 TW / beam, peak energies of ~25 kJ / beam (1053 nm), and pulse durations from a few hundred ps to 25 ns. Currently, four of the 192 beams have been completed, and have undergone testing for the past year.

NIF utilizes fiber amplifiers in the front end, and then approximately 130 optical components in each beamline after that. Optical modeling of this component system, from its nJ energies in the front end to kJ per beam on target, has been integral to designing the machine and helping to develop operating limits. In practice, this work has been separated into that work well-suited to ray-trace codes, and that which requires a diffraction code. For example, lens design, ghost analyses, and beam alignment calculations are done with ray models coupled with engineering drawings. Evaluations of issues such as nearfield beam modulation, beam energetics, and focal spot size are done with a diffraction code. This separation of tasks allows greater emphasis on component layout to be in the ray codes, and greater emphasis on issues such as laser gain and optics metrology to be placed in the propagation models. This paper will give a brief overview of the diffraction modeling work, and compare some recent results to predictions.

We will first discuss some physical effects which are included in the modeling, then the propagation code which is utilized, and finally compare some predictions to measurements.

2. PHYSICAL EFFECTS INCLUDED IN MODELING

Detailed diffraction modeling of a NIF beam must include several different physical effects and components. Of primary importance are gain, frequency conversion, the deformable mirror, and optical finishing (metrology).

2.1 Laser gain models

The heart of the laser system is the solid state gain media which amplifies the low-energy injected pulse. There are several amplification steps in a NIF beamline. These include the fiber amplifiers in the pulse forming network; a diode

laser pumped rod in the 60-pass regenerative amplifier (input nJ, output mJ); a flashlamp-pumped rod in the four-pass

* wwilliams@llnl.gov; phone: 925-423-1945; fax 925-423-6692

preamplifier stage (input mJ, output J); and flashlamp-pumped slabs in the main and power amplifiers (input J, output kJ), which are passed four or two times, respectively. The regenerative amplifier rod is 5 mm diameter x 50 mm long; the preamplifier rod is 50 mm diameter x 480 mm long; both are Nd-doped phosphate glass. The laser slabs in the main and power amplifiers are approximately 450 x 800 x 40 mm in size, and are also Nd-doped phosphate[1]. The slabs are mounted at Brewster's angle, allowing a square beam.

The laser propagation models typically start with the regenerative amplifier. They include the spatial dependence of the gain depletion by the laser beam. To do this the models require the spatially-dependent gain profile created by the pumping. For the regenerative amplifier, pumped by diodes, this profile is considered to be uniform, with a gain of ~1.8 per pass. For the preamplifier rod we use a measured gain profile, which is approximately parabolic in shape, with a gain of ~10 per pass.

For the laser slabs we have used both calculated and measured pumped profiles. The calculated profiles result from detailed ray trace calculations from the flashlamps to the laser slabs. A resulting calculated gain profile is compared in Figure 1 with results from early NIF prototype measurements.

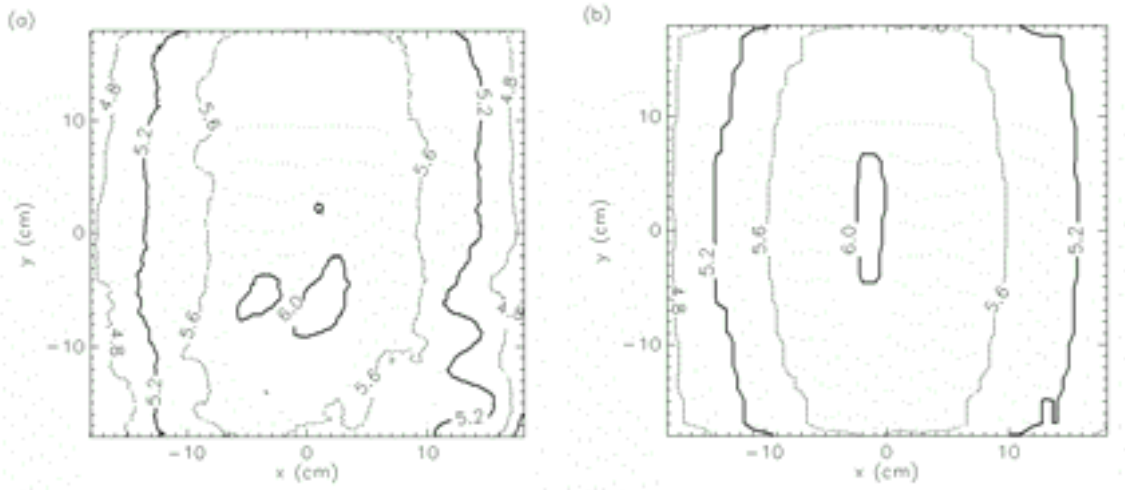

Figure 1. A comparison of measured (a) and calculated (b) gain profiles for a laser slab (in units of %/cm).

2.2 Frequency conversion model

Some NIF experiments will utilize frequency-converted light. The frequency converter for each beamline is mounted on the target chamber. Frequency conversion is accomplished using two thin, large crystal plates (~400 x 400 x 10 mm), through which the beam passes (see Figure 2)[2]. In the first plate, made of KH_2PO_4 (KDP) the laser light at 1053 nm is partially converted to a mix of 1053 nm and 531 nm light. In the second crystal, made of deuterated KDP, this mix of 1ω and 2ω is converted to 351 nm light (3ω) with attained conversion efficiencies of 70-80%.

Our models of frequency conversion include the basic equations of frequency conversion[3], as well as such details as the crystal index uniformity, bulk absorption, surface finish quality, diffraction, stress-optic effects, laser bandwidth, dispersion, non-linear index of refraction, and beam spatial and temporal uniformity. Taking these into account allows for good agreement between measured and calculated frequency conversion efficiencies on NIF (see Figure 3).

2.3 Deformable mirror model

Each beamline in NIF will have one 39-actuator deformable mirror[4] at the full beam size. This component serves the important purpose of flattening the wavefront to correct for imperfections in the optics (especially coating-induced

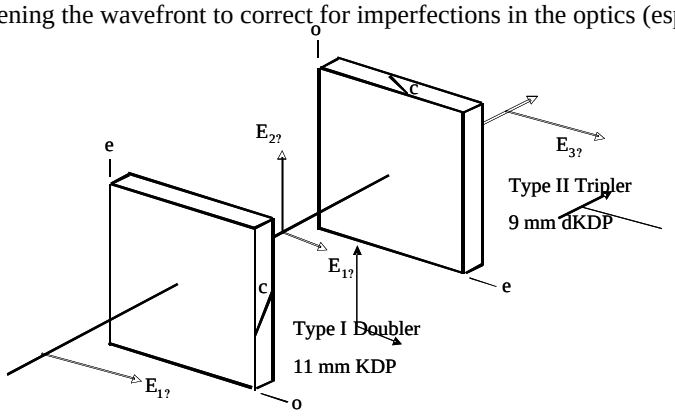

Figure 2. The NIF frequency converter consists of one KDP and one dKDP plate with the crystal axes such that 1053 nm light is efficiently converted to 351 nm light

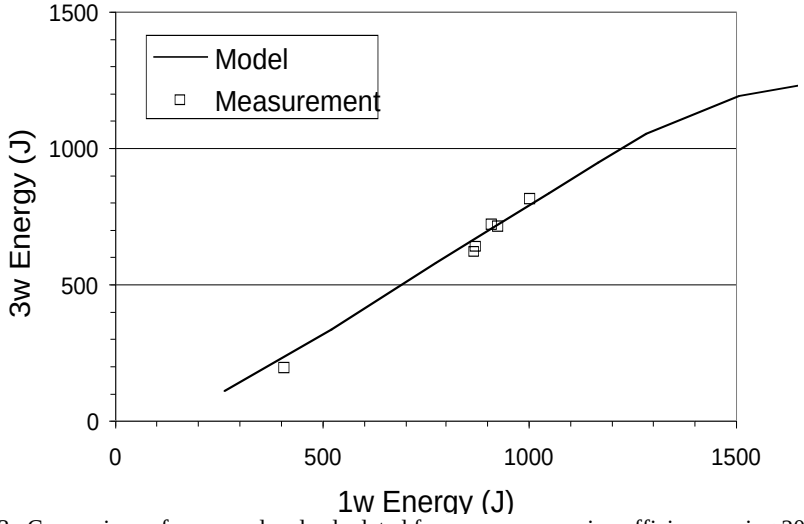

Figure 3. Comparison of measured and calculated frequency conversion efficiency using 200 ps FWHM Gaussian pulses on NIF.

curvature on mirrors and polarizers). More importantly, it corrects a large, approximately cylindrical wavefront induced on the beam by the flashlamp pumping of the amplifier slabs. As the slabs are pumped (over a few hundred μs) they undergo bending moments and index changes due to the non-uniform heating which results. This induces a wavefront on the beam of ~8 waves (1053 nm) P-V from the approximately 50 slab passes the laser sees. (This pump-induced distortion has been modeled in detail with good agreement between experiment and prediction[5].) The deformable mirror compensates effectively for this distortion, significantly improving the spot size on target.

The wavefront correction system employs a 77-lenslet Hartman sensor located in the output sensor diagnostic station, a fiber-optic wavefront reference source, and a feedback system. The wavefront reference generates a point source at the transport filter focal plane – equivalent to a nearfield plane wave in the laser and at the sensor. Lenslet focal-spot centroid displacements are measured with respect to this reference. By measuring the spot displacements that are generated when each actuator is pushed by a unit amount, and the spot displacements being generated due to the sensor beam aberrations, it is possible to predict the set of actuator movements that will generate a least-square minimization of

the net spot deviations. This correction process is carried out in a closed-loop system with 30 Hz operation and 3% feedback, yielding about a 1 second relaxation time.

Our calculational model of wavefront control closely follows the physical system. Measured influence functions – the mirror shape distortion generated by unit displacement of each actuator – generate a model of the wavefront an otherwise-perfect beam would have at the Hartman sensor. This beam is masked by the aperture of each of the lenslets, and the centroids of the focal spots are calculated, yielding the influence matrix. Measured component metrology is coupled with calculated pump-induced thermal slab distortion effects to predict the beam wavefront at the sensor, and the associated lenslet spot displacements. Singular value decomposition of the influence matrix then predicts the actuator pushes necessary to minimize the root-sum-square of the spot displacements. The resulting mirror shape is generated as a linear sum of influence functions, and this shape is used to predict shot-time beam propagation, energy extraction, and target-chamber focusing properties.

2.4 Optics Metrology

All the large aperture optics for NIF (approximately 40 per beamline) are inspected using full-aperture interferometry as part of the procurement process. These interferograms are available for use directly in the propagation modeling, and have been utilized for the four currently-completed beamlines. An example of one such interferogram is shown in Figure 4. The spatial resolution in these images is about 0.4 mm. This allows full-beam simulations, which are typically done with a spatial resolution of 1 mm, to include many of the physical effects of interest due to wavefront non-uniformities: beam intensity modulations due to diffraction, focal spot sizes, deformable mirror loading, and pinhole clipping in the spatial filters.

In addition, representative high-resolution surface metrology is available for all large optics. This information is used in modeling of small patches of the beam.

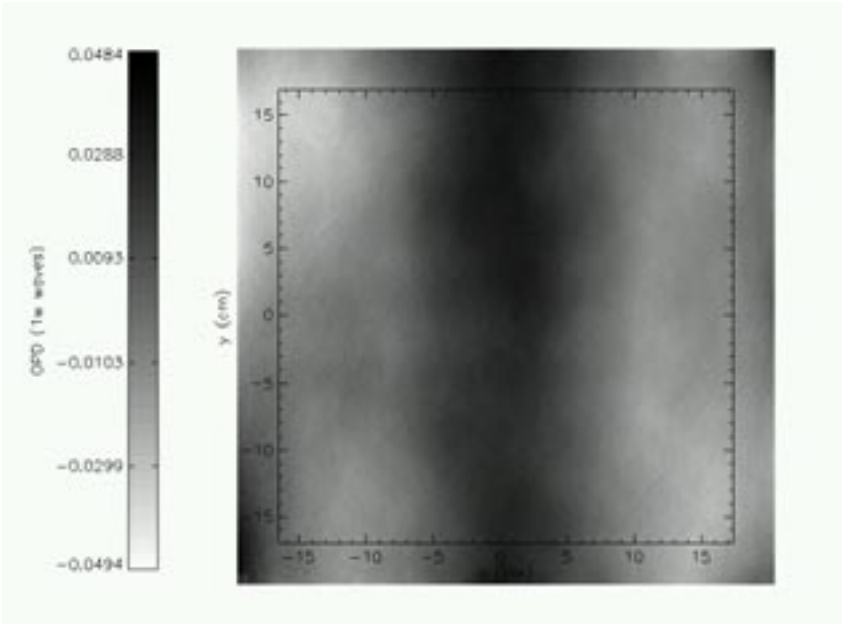

Figure 4. An example of the full-aperture interferometry information used in the propagation models (a laser slab transmitted wavefront).

3. THE PROPAGATION CODE

The principle propagation model used in the last 10 years of NIF design and construction has been a diffraction code developed here at LLNL called “PROP” (previously, “PROP92”). The code was developed specifically to model the

types of optical components and physics regimes we encounter in high-power fusion lasers. In general, it describes the laser beam as an electric field, $\boldsymbol{E}(x,y,z,t)$ on a rectangular spatial grid, using a fast Fourier transform for propagation. Details of the code have been reviewed elsewhere[6]. Aspects of the code specifically pertinent to NIF are briefly summarized here:

Vacuum propagation: PROP is a paraxial, Fourier code. Propagation in a linear, homogeneous medium is performed as follows: a) Fourier transform, b) multiply each Fourier component by a propagation phase, and c) inverse Fourier transform.

Nonlinear propagation: Typical optical materials have an intensity-dependent component of the index of refraction. For propagation through these materials short propagation steps are taken, followed by the addition of a phase proportional to the intensity at each point in the spatial grid.

Gain elements: Gain is treated using the Frantz-Nodvik formulas[7]. This formalism integrates out the temporal dependence of the laser pulse in energy extraction calculations, and is valid for pulses short compared to the pumping and spontaneous emission times. It allows us to model the temporal pulse shape with minimal resolution, while still calculating energy amplification correctly. The thickness of the gain element is split into (typically) a few sub-slices. In each sub-slice the beam is propagated, intensity-dependent phase is added, and the gain calculations are performed.

Optical aberrations: Spatially-resolved phase aberrations from optical metrology, pump-induced distortion, and the deformable mirror correction are added to the electric field.

Spatial filters: An important component of high power lasers is the spatial filter, which is physically a pinhole at the focal point of a pair of lenses. This pinhole serves to scrape off high-spatial-frequency components in the electric field, which tend to undergo higher non-linear growth in nonlinear propagation, causing large beam modulation and subsequent damage to optics at high power. NIF has two large spatial filters in each beamline, one 22 m long, and the other 60 m long. Each has a pinhole of 100 – 200 μrad (the ratio of the pinhole radius to the lens focal length). PROP models a spatial filter by performing a Fourier transform on the electric field, then removing all energy outside the specified radius.

4. MODEL COMPARISON TO DATA

A detailed propagation model of each beamline of NIF, using PROP, is run prior to every laser shot in order to develop the shot setup injection pulse shapes and energies, as well as predicting damage risks to optics from possible high fluences. This code package, called the Laser Performance Operations Model, is detailed elsewhere in these proceedings. With these predictions, detailed comparisons to data can be done for each shot. Below are sample comparisons of beam nearfield, farfield, and temporal shape.

4.1 Nearfield

A nearfield comparison of model predictions and data is shown in Figure 5. This shot was 16.6 kJ / beam (1ω) in a 10 ns temporally-flat pulse. The fine-scale structure on the beam is driven by optics finishing imperfections. Even with the use of actual optics metrology in our models, with the presence of so many optics in each beam we do not attempt to match the details of this structure in the data. Rather, we make a statistical comparison, typically given by the beam contrast, which is defined as the rms around the mean, divided by the mean. In this case the high-frequency contrast for the measurement over the central 30 x 30 cm was 5.8%, while that for the calculation was 6.3%.

4.2 Farfield

A 1ω farfield comparison of model predictions and data is shown Figure 6. Figure 6a shows the measured focal spot. Figure 6b is the model prediction for the same output energy. These images are intended to represent the same distance from the focus lens (close to, but not at best-focus), although measurement uncertainties make this difficult to ascertain accurately. Figure 6c shows a radial energy integral centered on the beam centroid, showing good agreement.

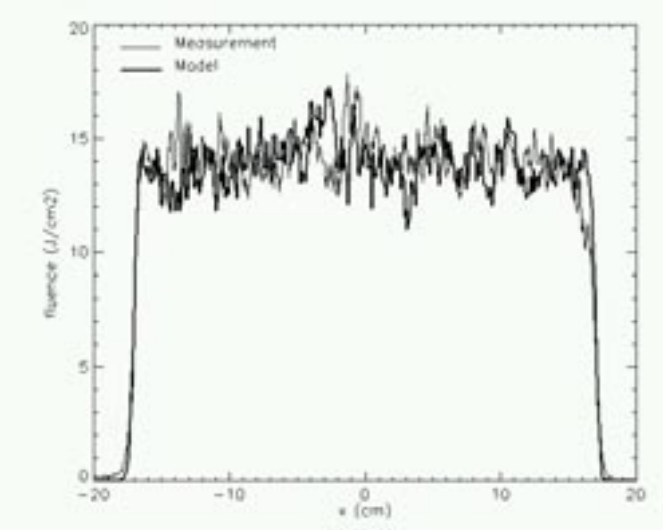

Figure 5. A lineout through measured and modeled nearfields. The propagation modeling does not attempt to match the fine-scale structure in the measurement exactly.

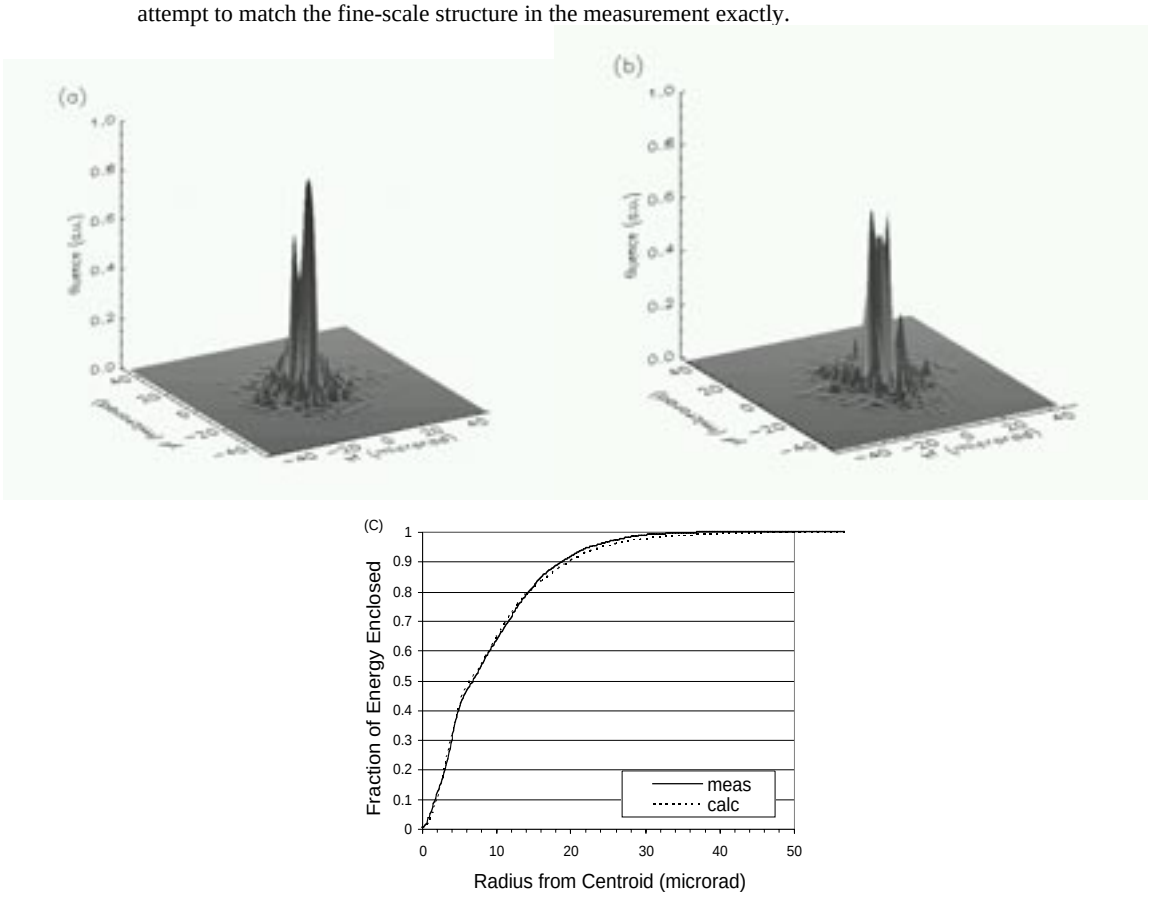

Figure 6. A comparison of measured (a) and calculated (b) farfields at a plane near best focus. The fractions of energy enclosed as a function of distance from the centroid agree well (c).

4.3 Temporal

The ability of the propagation models to predict the change in temporal pulse shape due to gain saturation is shown in Figure 7 for a 12.7 kJ (1ω) shot. Figure 7a is the pulse leaving the 4-pass rod amplifier; Figure 7b is the pulse at the end of the laser.

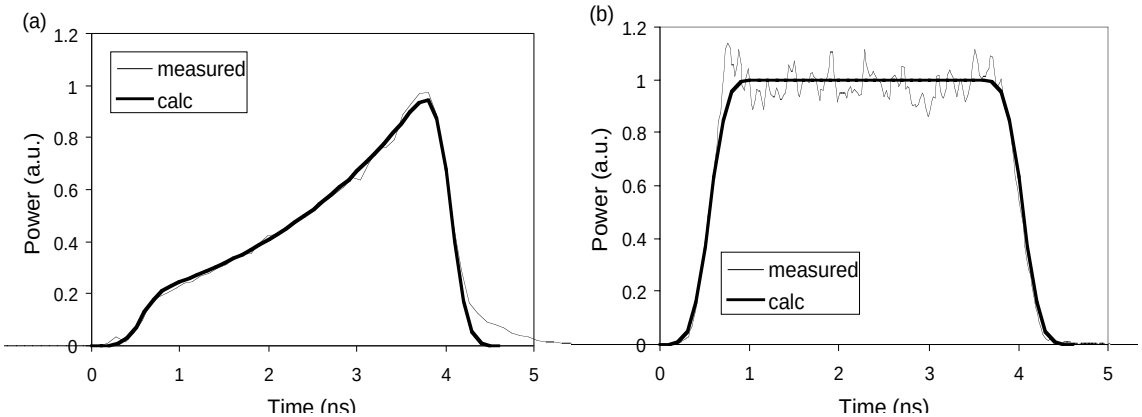

Figure 7. A comparison of the predicted and measured temporal pulse shape at the output of the 4-pass rod (a) and the output of the main 1ωlaser (b).

REFERENCES

1. Campbell JH, Suratwala TI, Thorsness CB, Hayden JS, Thorne AJ, Cimino JM, Marker AJ, Takeuchi K, Smolley M, Ficini-Dorn GF, "Continuous melting of phosphate laser glasses.", *Journal of Non-Crystalline Solids.* **263(1-4):**342-357, 2000 Mar.

2. Jim De Yoreo, Alan Burnham, Pam Whitman, "Developing KDP and DKDP crystals for the world's most powerful laser," *International Materials Review* Vol **47(3)**,113 - 152 (2002).

3. Jerome M. Auerbach, Paul J. Wegner, Scott A. Couture, David Eimerl, Robin L. Hibbard, David Milam, Mary A. Norton, Pamela K. Whitman, Lloyd A. Hackel, "Modeling of frequency doubling and tripling with measured crystal spatial refractive-index nonuniformities", *Applied Optics*, **40(9):**1404-1411 (20 March 2001).

4. Zacharias, Richard A.; Bliss, Erlan S.; Winters, Scott; Sacks, Richard A.; Feldman, Mark; Grey, Andrew; Koch, Jeffrey A.; Stolz, Christopher J.; Toeppen, John S.; Van Atta, Lewis; Woods, Bruce W., "Wavefront control of high-power laser beams in the National Ignition Facility (NIF)", Proc. SPIE Vol. 3889, p. 332-343, Advanced High-Power Lasers, Marek Osinski; Howard T. Powell; Koichi Toyoda; Eds., Osaka Japan, April, 2000.

5. Mark Rotter, Ken Jancaitis, Chris Marshall, Luis Zapata, Al Erlandson, Geoffroy LeTouze, Stephane Seznec, "Pump-Induced Wavefront Distortion in Prototypical NIF/LMJ Amplifiers – Modeling and Comparison with Experiments", Proc. 3rd Intl. Conf. on Solid State Lasers for Application to Inertial Confinement Fusion, SPIE Vol. 3492, pg. 638-659.

6. R. A. Sacks, M. A. Henesian, S. W. Haney, and J. B. Trenholme, "The PROP92 Fourier beam propagation code," *ICF Annual Report*, UCRL-LR-105821-96, 1996, p. 207

7. L.M. Frantz, J.N. Nodvik, *J. Appl. Phys*. **34(8),** 2346-2349 (1963).